Path Tracking Control for Micro-robots with Helmholtz-Maxwell Coils Actuation

Daniel F. Murcia Rivera(✉) and Hernando Leon-Rodriguez(✉)

Industrial and Mechatronics Engineering Departments, Faculty of Engineering, Nueva Granada Military University, Bogota, Colombia
{ul802440,hernando.leon}@unimilitar.edu.co

Abstract. This work is dedicated to present a proposed control system for tridimensional and planar position of a magnetized micro-robot on a high viscous medium with electromagnetic actuation. Detailed process for control derivation, simulation and experiments are exposed.

Keywords: Micro-robot · Path tracking · Electromagnetic actuation · Discrete control

1 Introduction

The physics at low-level scale can become weird compared to macro-scale because the appearance of forces and effects that where despised on macro-scale. Micro robots are systems that deal with this type of forces, and for many or partially all applications, it is required the control of position of them. Because of that, a prototype of a micro-robot relatively big with an electromagnetic actuator was developed.

The most highlighted application of these tiny systems, are related to health. Micro robots can treat blocked vessels due to bad feeding or poor physical activity [1]. They can also deliver medicine into specific locations increasing the effectiveness of the medicine and reducing secondary effects in other body parts [2]. Endoscopy is another area of application, [3] and [4] develop electromagnetic systems for specialized endoscopy micro robots. Comparing with traditional methods, this technology can overcome issues of infection due to surroundings [5] and risks due to competence [6].

The first thing to consider at these scales is the dominance of viscous forces. The Reynols number in this domain become small and by its definition, it indicated that it can be despised the inertial forces. The movement of the robot becomes no past dependent, and only determined by forces applied at the instant [7]. The system of this article is not fully at micro-scale, so perhaps consideration of its forces is necessary.

Another issue of these tiny systems is how to implement the actuator that generates the movement. Firstly, the power supply, in macro-scale batteries are used but using this at tiny scale results on big complexity [8]. Second, if is actually fulfilled the energy issue, how the actuator can transform its supply into kinetic energy? Complex machining processes are necessary for creating the actuator. A system for delivering medicine show on [9] uses a micro-hydraulic pump actuator.

J. C. Figueroa-García et al. (Eds.): WEA 2019, CCIS 1052, pp. 64–77, 2019.
https://doi.org/10.1007/978-3-030-31019-6_6

The approach in the presented system is to manage the actuation by an electromagnetic generator exercising forces over a magnetized robot. The complexity of tiny actuators is simplified but control becomes complex because of nonlinearities. Electromagnetic actuation systems are diverse, categorizing them there are two class of actuation: gradient and rotatory magnetic field [10]. In case of the type of electromagnetic generator, there are permanent magnet and coil magnet types [11]. Figures 1 and 2 shown the used actuation system based in coils generators producing both class of actuation, [12] presents a similar system.

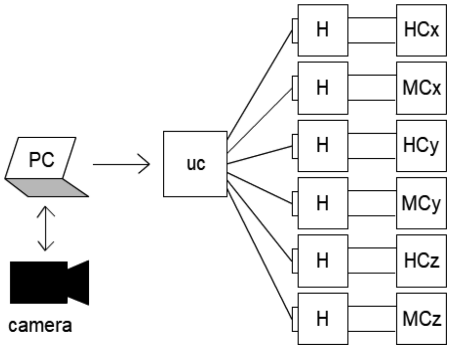

Fig. 1. Schematic micro-robot system diagram uc: microcontroller H: h bridge circuit HC: Helmholtz coil MC: Maxwell coil

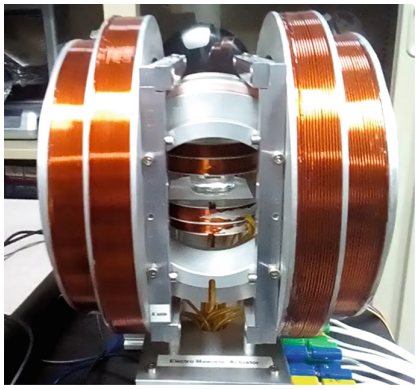

Fig. 2. Implemented electromagnetic actuation system

2 System and Equipment

The based equipment used to evaluate the trajectory of the micro robots are one Camera Canon EOS Rebel T3 1100D with Macro Lens 100 mm; 6 DC Power supply Versatile Power BENCH 100-10XR. Table 1 is showing the geometry and parameter of each coil placed in the axis x, y, z; and also the number of coil's turns

Table 1. System geometry and coils parameters.

Coils	Axis	Diameter (mm)	N turns
Helmholtz	x	200	196
	y	121.5	234
	z	65	221
Maxwell	x	172	240
	y	114	320
	z	61	165

3 Modelling

3.1 Three-Dimensional Space Model

Equations (1) and (2), presented by [12], govern the way an intensity magnetic field $\vec{H}$ influence over the dynamics of a permanent magnet.

$$\vec{F} = \mu_0 V(\vec{M} \cdot \nabla)\vec{H} \tag{1}$$

$$\vec{T} = \mu_0 V\vec{M} \times \vec{H} \tag{2}$$

Rewriting (1) by expanding the operation result in:

$$\vec{F} = \mu_0 V\left(M_x \frac{\partial \vec{H}}{\partial x} + M_y \frac{\partial \vec{H}}{\partial y} + M_z \frac{\partial \vec{H}}{\partial z}\right)$$

By using the principle of superposition, the total H field is the sum of the field produced by Maxwell ($\overrightarrow{H_m}$) and Helmholtz ($\overrightarrow{H_h}$) coils.

$$\vec{H} = \overrightarrow{H_m} + \overrightarrow{H_h} \tag{3}$$

Please note that the first paragraph of a section or subsection is not indented. The first paragraphs that follows a table, figure, equation etc. does not have an indent, either.

Subsequent paragraphs, however, are indented.

3.2 Independence of Force Under the Influence of Helmholtz Coils

Defining a new vector $\overrightarrow{\partial_p H_m}$ the H field is:

$$\overrightarrow{H_m} = \overrightarrow{\partial_p H_m} \circ [x \quad y \quad z]^T \tag{4}$$

Because $\overrightarrow{\boldsymbol{H_m}}$ is a gradient field, and $\overrightarrow{\boldsymbol{H_h}}$ is a uniform field, only $\overrightarrow{\boldsymbol{H_m}}$ has incidence over the actuation force.

$$\frac{\partial \overrightarrow{H_m}}{\partial v} = \left[\frac{\partial \overrightarrow{H_m}}{\partial x} \quad \frac{\partial \overrightarrow{H_m}}{\partial y} \quad \frac{\partial \overrightarrow{H_m}}{\partial z}\right]^T$$

$$\frac{\partial \overrightarrow{H_m}}{\partial v} = \overrightarrow{\partial_p H_m} \qquad \frac{\partial \overrightarrow{H_h}}{\partial v} = 0$$

Using (3) and the expand form of (1), the actuation force is:

$$\vec{F} = \mu_0 V[\, M_x \partial_x H_{mx} \quad M_y \partial_y H_{my} \quad M_z \partial_z H_{mz}\,]^T$$

$$\vec{F} = \mu_0 V\left(\vec{M} \circ \overrightarrow{\partial_p H_m}\right) \tag{5}$$

Note that v express a system coordinate variables (x, y, z) and that $\circ$ corresponds to the Hadamart product.

3.3 Planar Space Model

In planar space, the actuation force $\vec{F}'$ is given by replacing with local variables $\vec{M}'$ and $\overrightarrow{\partial_p H'_m}$ on (5) that are characterized for having zero components on $\hat{z}'$. The actuation torque is simply the z component of (2) with local variables.

$$\vec{F}' = \mu_0 V\left(\vec{M}' \circ \overrightarrow{\partial_p H'_m}\right)$$

$$T' = \mu_0 V[\,0 \quad 0 \quad 1\,]\vec{M}' \times \vec{H}'$$

Introducing dynamics of the magnetic body and its medium, the proposed dynamic model is:

$$I\ddot{\theta}' = T' - B_i \dot{\theta}' \tag{6}$$

$$m\ddot{\vec{p}}' = \vec{F}' - B_f \dot{\vec{p}}' - \vec{W} \tag{7}$$

Depending on size, weight ($\vec{W}$) can be despised.

3.4 Coils Field as Function of Currents

Theory exposed in [12] relates the coils current and the H field generated for both Helmholtz and Maxwell coils.

$$\overrightarrow{I_m} = \begin{bmatrix} i_{m1} \\ i_{m2} \\ i_{m3} \end{bmatrix} \tag{8}$$

For Maxwell case, defining a current vector (8) for enclosing coils current in one variable is necessary to rewrite equations in matrix form.

$$\overline{C_m} = 0.6413 \begin{bmatrix} n_{m1} r_{m1}^{-2} & 0 & 0 \\ 0 & n_{m2} r_{m2}^{-2} & 0 \\ 0 & 0 & n_{m3} r_{m3}^{-2} \end{bmatrix} \tag{9}$$

$$\bar{G} = \begin{bmatrix} 1 & -0.5 & -0.5 \\ -0.5 & 1 & -0.5 \\ -0.5 & -0.5 & 1 \end{bmatrix} \tag{10}$$

From these matrix variables the equations relating current and gradient field for Maxwell coils are:

$$\overrightarrow{g_m} = \overline{C_m}\overrightarrow{I_m} \tag{11}$$

$$\overrightarrow{\partial_p H_m} = \bar{G}\overrightarrow{g_m} \tag{12}$$

Helmholtz coils equations can also rewritten into matrix form, where its current vector is $\overrightarrow{I_h}$.

$$\overrightarrow{H_h} = 0.7155\left[\frac{n_{h1}}{r_{h1}} \quad \frac{n_{h2}}{r_{h2}} \quad \frac{n_{h3}}{r_{h3}}\right]^T \circ \overrightarrow{I_h} \tag{13}$$

3.5 Maxwell Coils Influence on Orientation

As [12] mentioned, the orientation of the magnet is controlled by Helmholtz coils. From (6) the result system is:

$$I\ddot{\theta}' = \mu_0 VM\left(H'_y cos(\theta') - H'_x sin(\theta')\right) - B_i\dot{\theta}'$$

Making dynamic variables zero the steady condition of the system is:

$$H'_y cos(\theta') = H'_x sin(\theta')$$

$$\left|\overrightarrow{H'}\right| sin\left(\theta'_d\right) cos(\theta') = \left|\overrightarrow{H'}\right| cos\left(\theta'_d\right) sin(\theta')$$

$$\theta'_d = \theta'$$

Which means that actual magnet's orientation will match H field orientation if is applied a magnitude of field different to zero. However considering (3) the $\overrightarrow{H'}$ will include $\overrightarrow{H'_m}$ that is not constant and is function of the actual position, causing an undesirable deviation of the induced orientation by the Helmholtz coils.

3.6 About Approximations

The exposed model for the calculation of the H field generated by the coils is valid along some limits of operation. It is important to take into account these restrictions for understanding the parameters of the controller.

$$\oint \vec{H} d\vec{s} = I + \iint \vec{D} d\vec{f} \tag{14}$$

The physical law for electromagnetics is mainly Maxwell's equations, from where Biot-Savart's law can derived from (14) by approximating D to zero, which is valid for DC current [13]. This statement points out limits of frequency for the actuator signals, been slow changes more accurate than fastest.

$$B(z) = \frac{\mu_0 I n r^2}{2} \left[\frac{1}{\left(r^2 + \left(z - \frac{d}{2}\right)^2\right)^{3/2}} \pm \frac{1}{\left(r^2 + \left(z + \frac{d}{2}\right)^2\right)^{3/2}} \right] \tag{15}$$

The magnetic field of a point along the z-axis of a coil pair exposed by [14] is compacted on (15), where the plus sign correspond to Helmholtz and minus to Maxwell coil. The model expressions (12) and (13) are obtained evaluating the function of the magnetic field at z = 0, in the case of Maxwell coil the approximation is done by Taylor series expansion (order one) for the function at point z = 0. Therefore, the model operation point is [0 0 0] and is valid for points near to it.

The estimates constants are computed as follow:

$$\mu_0 = 2.3709 * 10^{-8} \frac{\mathrm{H}}{\mathrm{m}}$$

$$V = 2.5133 * 10^{-8}\,\mathrm{m}^3$$

$$M = 50 * 10^{6} \frac{\mathrm{A}}{\mathrm{m}}$$

$$B_f = 0.1964 \frac{\mathrm{Ns}}{\mathrm{m}}$$

$$B_i = 4.0 * 10^{-6} \frac{\mathrm{Nms}}{\mathrm{rad}}$$

4 Control

4.1 Variable Planar Space

A variable planar space is proposed for simplify the tridimensional position control. In this approach the actual position and the actual desired point resides in a plane. The initial magnetization vector $\overrightarrow{M_0}$ and the target vector $\overrightarrow{T_A}$, that aims the desired position $\overrightarrow{P_d}$, defines the basis vectors for the planar subspace.

$$\overrightarrow{T_A} = \overrightarrow{P_d} - \overrightarrow{P_0} \tag{16}$$

$$\hat{x}' = \frac{\overrightarrow{M_0}}{\left\|\overrightarrow{M_0}\right\|} \qquad \hat{z}' = \frac{\overrightarrow{M_0} \times \overrightarrow{T_A}}{\left\|\overrightarrow{M_0} \times \overrightarrow{T_A}\right\|} \tag{17}$$

Rotating $\hat{x}'$ by 90º over the $\hat{z}'$ axis by applying Rodrigues rotation formula, the final basis is then:

$$\hat{y}' = \hat{z}' \times \hat{x}' + \hat{z}'(\hat{z}' \cdot \hat{x}') \tag{18}$$

An indeterminate of the basis can be presented when the direction of $\overrightarrow{M_0}$ and $\overrightarrow{T_A}$ matches.

4.2 Maxwell Field

Finding $\overrightarrow{\partial_p H'_m}$ from the planar space model:

$$\overrightarrow{\partial_p H'_m} = \frac{\vec{F}'}{\mu_0 V} \circ \left(\vec{M}'\right)^{\circ -1}$$

By considering that robot's orientation is already the desired one then:

$$\angle \vec{F}' = \theta' \ \left|\vec{F}'\right| = F''$$

Defining a direction vector $\vec{a}$

$$\vec{a} = cos(\theta')\hat{x}' + \sin(\theta')\hat{y}'$$

Transforming into global coordinate system

$$\overrightarrow{\partial_p H_m} = \frac{F''\vec{a}}{\mu_0 V} \circ (M\vec{a})^{\circ -1}$$

Making the Hadamart power and product respect to the global basis vectors

$$\overrightarrow{\partial_p H_m} = \frac{F''}{\mu_0 VM}(\hat{x} + \hat{y} + \hat{z}) \tag{19}$$

If direction vector $\vec{a}$ has zero components, the corresponding component on $\overrightarrow{\partial_p H_m}$ is undefined and thus it can take any value, making (19) valid for any $\vec{a}$.

4.3 Gravity Compensation

The total force applied to the robot must compensate gravity for correct position control.

$$\vec{F} = \vec{F}' + \vec{W}$$

In consequence, on (19) is added an additional term

$$\overrightarrow{\partial_p H_m} = \frac{1}{\mu_0 VM}\left[F''(\hat{x}+\hat{y}+\hat{z}) + W\left(\hat{z} \circ (\vec{a})^{\circ -1}\right)\right]$$

Simplifying by discomposing vector $\vec{a}$, the resulting equation is only defined if z-component of $\vec{a}$ is different from cero.

$$\overrightarrow{\partial_p H_m} = \frac{1}{\mu_0 VM}\left[F''(\hat{x}+\hat{y}+\hat{z}) + Wa_z^{-1}\hat{z})\right] \tag{20}$$

4.4 Maxwell Currents

Using (11) and (12) the necessary current is:

$$\overrightarrow{I_m} = \left(\overline{GC_m}\right)^{-1}\overrightarrow{\partial_p H_m}$$

A problem finding current is that $\overline{G}$ is not invertible, so that cannot be achieved an arbitrary actuation force. Nevertheless, if movements are only at planes x-y, x-z or y-z, $\overline{G}$ $\overline{C_m}$ can be reduced to a submatrix ensuring the forces in plane and allowing neglecting the perpendicular force because components of $\vec{\mathrm{M}}$ cancel its influence.

$$\overrightarrow{I_m} = \left(\overline{GC_{sub}}\right)^{-1}\frac{1}{\mu_0 VM}\left[F''(\hat{x}+\hat{y}+\hat{z}) + Wa_z^{-1}\hat{z})\right] \tag{21}$$

4.5 Helmholtz Currents

$$\vec{H}' = \overrightarrow{H_m} + \overrightarrow{H_h} \tag{22}$$

For compensating Maxwell influence over the orientation of the robot, $\overrightarrow{H_h}$ should be set as (22) making local H stay in a desirable angle as $\overrightarrow{H_m}$ changes, as expressed on (4).

$$\angle \vec{H}' = \angle \overrightarrow{T'_A}$$

The requirement for this compensation is that direction must be corrected in continuous time because disorientation is also continuous. Therefore discrete control may not totally compensate Maxwell influence.

$$\overrightarrow{I_h} = 0.7155^{-1} \overrightarrow{H_h} \circ \left[\frac{r_{h1}}{n_{h1}} \quad \frac{r_{h2}}{n_{h2}} \quad \frac{r_{h3}}{n_{h3}} \right]^T \tag{23}$$

Increasing the magnitude of the field should reduce the undesired disorientation.

4.6 Discrete Control

$$m\ddot{p}'' = F'' - B\dot{p}'' \tag{24}$$

The model in the line that contains the actual and desired points is show on (24). Setting a state feedback discrete controller and if guaranteed desired orientation, the position of the robot is controlled.

$$q[k+1] = Gq[k] + Hu[k] \tag{25}$$

$$y[k] = Cq[k] + Du[k] \tag{26}$$

Equations (25) and (26) are the discrete state space representation of system (24), where: 'q' is the states vector, 'u' the input signal, and 'y' the output of the system.

Algorithm 1

$$u[k] = K_i v[k] - K\tilde{q}[k] \tag{27}$$

Algorithm 2

$$u[k] = sign(T_a \cdot T_{aa}[k]) abs(K_i v[k] - K\tilde{q}[k]) \tag{28}$$

An observer outputs an approximation for the state vector, this is denoted with $\tilde{q}$.

In one-dimensional space, the state vector 'q' includes velocity and position at this dimension. Distance from initial point to actual point (that is the position at this dimension) is always positive, so if disturbances make position go less than the inverse of the reference, Algorithm 1 will make unstable the system. Algorithm 2 takes into account actual target vector T_{aa} making system stable.

$$u[k] = F''[k] \tag{29}$$

$$v[k] = R[k] - y[k] + v[k-1] \tag{30}$$

$$\tilde{q}[k] = Hu[k-1] + Ly[k-1] + (G - LC)\tilde{q}[k-1] \tag{31}$$

With a settling time of 5 s and sampling time of 0.7 s the constants of the controller are:

$$K_i = 0.0486$$

$$K = [-0.0037 \quad 0.1808]$$

State observer constants:

$$L = \begin{bmatrix} 0 \\ 1 \end{bmatrix}$$

4.7 Point-to-Point Control Algorithm

Define initial $\overrightarrow{M_0}$, $\overrightarrow{P_0}$ vectors and calculate target vector $\overrightarrow{T_A}$. Define planar subspace basis defined on (17), (18). If $\angle\vec{M} \neq \angle\overrightarrow{T_A}$ orientation actuation is started using (23) and setting $\overrightarrow{H_h} = \widehat{T_a}$. When desired angle is reach, one-dimensional position control starts with (21) and (28). As desired orientation sets very fast, position control start in same time with orientation control. At each time step correct orientation by measuring the actual position, for compensating orientation disturbances. When desired position $\overrightarrow{P_d}$ is reach, move to next point starting again the control algorithm. When its position is inside a tolerance range, position $\overrightarrow{P_d}$ is reach.

5 Simulation

Simulation in Figs. 3 and 4 use 6-DOF equations of motion with respect to body axes, so a transformation from global to relative axes is necessary to convert forces to relative ones. Direction cosine matrix defines this transformation. Compensators are included to coincide the rigid body global system with used global system.

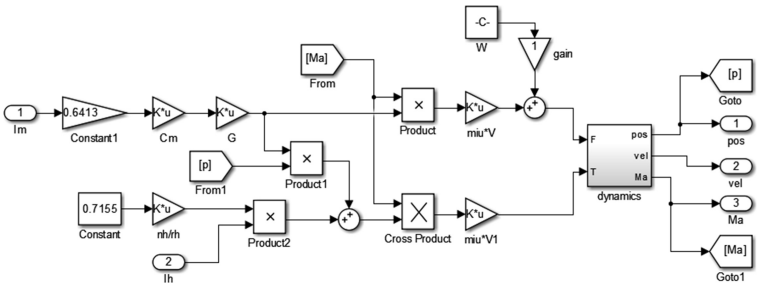

Fig. 3. Plant model. Current-forces conversion and gravity influence.

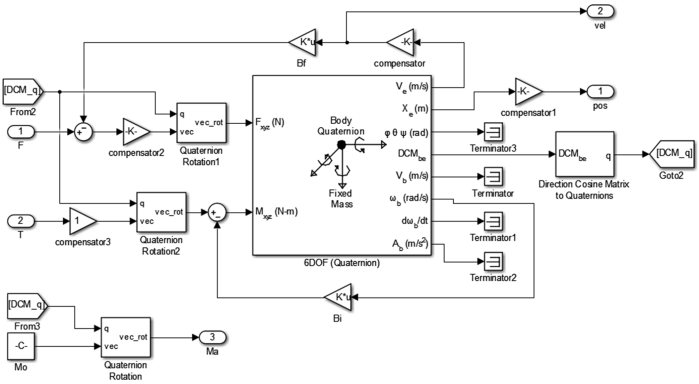

Fig. 4. Model. Dynamics of rigid body relating input forces-torques to position-orientation.

5.1 Saturation

Testing with saturation effect is presented in Figs. 5 and 6 as follows: Actual position [x, y, z] → [yellow, purple, aquamarine]; Reference position [x, y, z] → [red, green, blue].

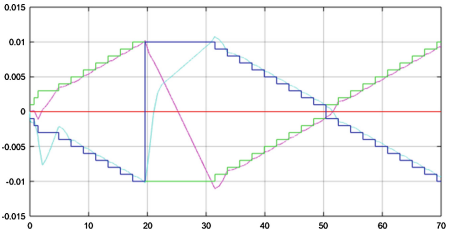

Fig. 5. Path 1 y-z plane. Position (m) versus time (s). (Color figure online)

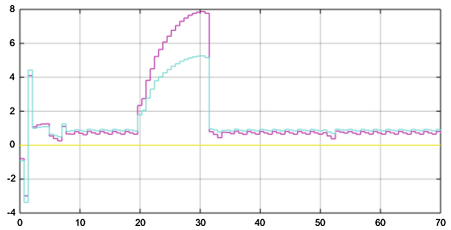

Fig. 6. Path 1. Current (A) versus time (s). Maxwell currents before saturation. (Color figure online)

Saturation is set to −2 and 2 A for the Maxwell currents. Relating Fig. 6 with 5, values that surpasses the saturation not fulfill gravity compensation on some intervals and spikes appear. On the other hand is expected, with no limits disturbance due to gravity on interval 0–5 s disappears and there is a reduction of time for reaching reference at 20–30 s.

5.2 Maxwell Influence

Maxwell influence and saturation is present and show in Figs. 7 and 8 can make the system not follow that good to the reference, by putting spikes. Reference changes as one-dimensional distance is reach even when position error remains. If Helmholtz currents are much larger than Maxwell's a decrease of Maxwell influence is done. The problem comes when Helmholtz current increase its approximation become less accuracy, Helmholtz coils begin to influence the actuation force showing in Fig. 8

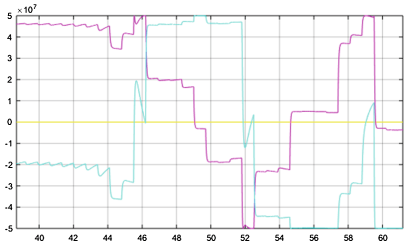

Fig. 7. Path 1. Orientation vector M (A/m) versus time (s)

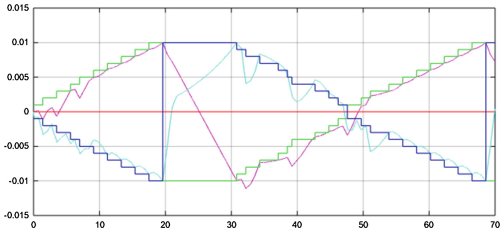

Fig. 8. Path 1. Position (m) versus time (s). Duplicated Hh magnitude.

5.3 Model Constants Error

Other errors of constants of model will affect control but the main constant that relates current and force will be priority as it determines the error of the control as show on Figs. 9 and 10, Which showing a result of axis error.

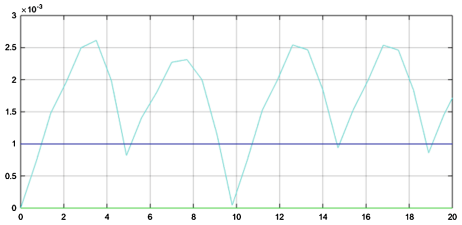

Fig. 9. Path 2. Position (m) versus time (s). Model constant uo*V with +10% of error

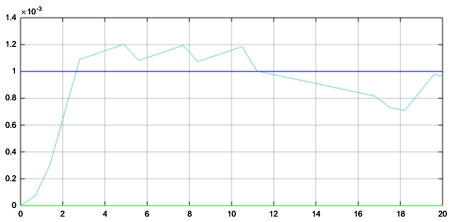

Fig. 10. Path 2. Position (m) versus time (s). Model constant Bf with +10% of error.

6 Results

Tested were carry out on x-y plane and these are represented as follow: Actual position [x, y] → [red, green]; Reference position [y, z] → [yellow, purple].

Figure 11 is showing a sequence of micro-robot trajectory and target positions. The blue crosses show some of the principal points set to be reach by the micro-robot creating a “S” trajectory.

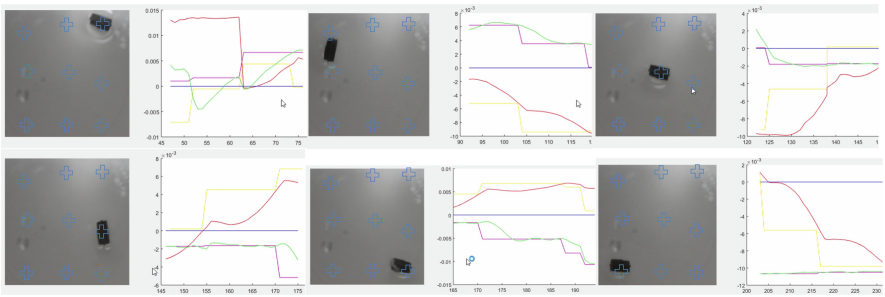

Fig. 11. Controller test. 'S' shape trajectory. Position (m) versus time (s). (Color figure online)

7 Conclusions

One of the limitations of the controller is that there is no correct gravity compensation while rotation occurs, only when desired orientation is reach compensation is correct. Also Maxwell influence sometimes causes high disorientations that cause spikes, plus quantization error and the saturation makes path tracking noisy. This a reason for little distortions present on Fig. 8. In addition, spikes on robot's position are as well cause of incomplete compensation at orientation z-values near zero the controller can improve if it implements a limit for angle orientation.

At implementation, spikes conduce system to instability probably because the inaccuracy of the model and the high non-linear behaviour of a magnetic levitating system that was tried to be done on 'z' axis. Therefore, is needed a more sophisticated control method for a robust control of 'z' position.

About x-y movement where gravity is not present, another non-linear problem emerges. Friction between robot and walls as well as changes on viscosity because wall-effects makes model observer not follow correctly the actual position causing that control do not work also at x-y when robot is at the bottom. By choosing a robot that can float in the surface of the medium, x-y control works well as presented.

On general 3D movement as explained on derivation of (21), allowed movements with its algorithms are only for certain planes. Also because disturbances and the lack of other feedback for full position measurement, 3D movement will tend to be incorrect as disturbances and errors accumulates. Also is important to remark the importance of characterization because model constants error will affect the effectiveness of the controller.

For future works and for enabling a full 3D path a solution can be from taking multi-point approximations and variable controller constants as well a more accurate and sophisticated observer that takes in account non-linear disturbances affected the robot.

Acknowledgement. This research was supported by the project Inv-Ing-2106 Nueva Granada Military University of Colombia.

References

1. Park, S., Cha, K., Park, J.-O.: Development of biomedical microrobot for intravascular therapy. Int. J. Adv. Robot. Syst. **7** (2010). https://doi.org/10.5772/7260
2. Nelson, B., Kaliakatsos, I., Abbott, J.: Microrobots for minimally invasive medicine. Ann. Rev. Biomed. Eng. **12**, 55–85 (2010). https://doi.org/10.1146/annurev-bioeng-010510-103409
3. Yim, S., Sitti, M.: Design and rolling locomotion of a magnetically actuated soft capsule endoscope (2012)
4. Ciuti, G., Valdastri, P., Menciassi, A., Dario, P.: Robotic magnetic steering and locomotion of capsule endoscope (2009)
5. Cowen, A.: The clinical risks of infection (2001)
6. Romagnuolo, J., Cotton, P., Eisen, G., Vargo, J., Petersen, B.: Identifying and reporting risk factors for adverse events in endoscopy (2011)
7. Purcell, E.M.: Life at Low Reynolds Number. AIP Publishing (1976)
8. Choi, H., et al.: Electromagnetic actuation system for locomotive intravascular therapeutic microrobot (2014)
9. Ha, V.L., et al.: Novel active locomotive capsule endoscope with micro-hydraulic pump for drug delivery function (2016)
10. Jeong, S., Choi, H., Young, S.K., Park, J.-O., Park, S.: Remote controlled micro-robots using electromagnetic actuation (2012)
11. Xu, T., Yu, J., Yan, X., Choi, H., Zhang, L.: Magnetic actuation based motion control for microrobots (2015)
12. Lee, C., et al.: Helical motion and 2D locomotion of magnetic capsule endoscope using precessional and gradient magnetic field (2014)
13. PHYWE series of publications: Magnetic field of paired coils in Helmholtz arrangement, Göttingen, Germany
14. Youk, H.: Numerical study of quadrupole magnetic traps for neutral atoms: anti-Helmholtz coils and a U-chip. Can. Undergraduate Phys. J. **3**, 13–18 (2005)